





Barium titanate-enhanced hexagonal boron nitride inks for printable high-performance dielectrics

Hyunho Kim¹ , Adrees Arbab^{1,2}, Benji Fenech-Salerno¹ ,
Chengning Yao¹ , Ryan Macpherson¹, Jong Min Kim² and
Felice Torrisi^{1,3} 

¹Molecular Sciences Research Hub, Department of Chemistry, Imperial College London, White City Campus, 82 Wood Lane, London W12 0BZ, United Kingdom

²Department of Engineering, University of Cambridge, 9 JJ Thompson Avenue, Cambridge CB3 0FA, United Kingdom

³Dipartimento di Fisica e Astronomia, Università di Catania, Via S. Sofia, 64, 95123, Catania, Italy

E-mail: f.torrisi@imperial.ac.uk

Received 17 November 2021, revised 7 February 2022

Accepted for publication 15 February 2022

Published 4 March 2022



CrossMark

Abstract

Printed electronics have been attracting significant interest for their potential to enable flexible and wearable electronic applications. Together with printable semiconductors, solution-processed dielectric inks are key in enabling low-power and high-performance printed electronics. In the quest for suitable dielectrics inks, two-dimensional materials such as hexagonal boron nitride (h-BN) have emerged in the form of printable dielectrics. In this work, we report barium titanate (BaTiO₃) nanoparticles as an effective additive for inkjet-printable h-BN inks. The resulting inkjet printed BaTiO₃/h-BN thin films reach a dielectric constant (ϵ_r) of ~ 16 by adding 10% of BaTiO₃ nanoparticles (in their volume fraction to the exfoliated h-BN flakes) in water-based inks. This result enabled all-inkjet printed flexible capacitors with $C \sim 10.39 \text{ nF cm}^{-2}$, paving the way to future low power, printed and flexible electronics.

Supplementary material for this article is available [online](#)

Keywords: printed electronics, dielectrics, inkjet printing, hexagonal boron nitride, barium titanate nanoparticle


(Some figures may appear in colour only in the online journal)

1. Introduction

Printed electronics has the potential to enable low-power, large scale flexible electronics [1]. Low operation voltages ($<5 \text{ V}$), thin films ($<10 \mu\text{m}$) and solution processable materials are key to achieving high-performance printed and flexible electronic components [2, 3]. Active electronic

devices are normally composed of a semiconductor, a conductor, and a dielectric material.

While a lot of effort has been placed in the development of solution-processed semiconductors with high mobility and on/off current ratio, printable dielectric inks are relatively less investigated. Thin films of printed nanomaterials often suffer from existing pinholes which results in relatively low breakdown strengths (B_v) of $<1 \text{ MV m}^{-1}$. Organic dielectrics can offer higher B_v but lower dielectric constant (ϵ_r). It is challenging to achieve high-performance printed electronics, and these limit the establishment of all printed electronic components such as field-effect transistors and energy storage devices.

 Original content from this work may be used under the terms of the [Creative Commons Attribution 4.0 licence](#). Any further distribution of this work must maintain attribution to the author(s) and the title of the work, journal citation and DOI.

Printable dielectrics have been developed by using cross-linked polymer blends such as poly(4-vinyl)phenol and silane reagents, achieving $\epsilon_r \sim 5.7$ and $B_v \sim 3\text{--}6 \text{ MV cm}^{-1}$ [4]. Recently, nanomaterials have been used in the form of additives or conductive fillers to improve the dielectric properties. Gold nanoparticles have been grafted with thiol-terminated polystyrene, resulting in printed dielectric films achieving $\epsilon_r \sim 50$ and $B_v \sim 39.1 \text{ MV m}^{-1}$ [5]. On the other hand, high ϵ_r nanoparticles such as barium titanate (BaTiO_3) can be considered for higher dielectric performance. For example, nanocomposite of BaTiO_3 and poly(vinylidene fluoride-co-hexafluoro propylene) dielectric thin films show $\epsilon_r \sim 20$ and $B_v \sim 260 \text{ MV m}^{-1}$ [6]. BaTiO_3 is one of the most used dielectric materials with a high ϵ_r of around 500 at room temperature [7]. This is due to their perovskite structure where a central Ti atom can make a large displacement under an external electric field. BaTiO_3 is one of the key materials in the application of multi-layer ceramic capacitors [8], while their use as gate dielectrics is much less studied in detail.

Inks based on two-dimensional (2D) materials have been demonstrated to be a suitable platform for printed electronics [9], with the charge transport dominated by the inter-flake or intra-flake hopping [10]. Large scale production of 2D materials by liquid-phase exfoliation [11], microfluidic exfoliation [12], or electrochemical exfoliation (EE) [13] yields few-layer 2D material inks for electronics, with conducting (e.g. MXenes) [14], semiconducting (e.g. transition metal dichalcogenides) [15, 16], and insulating properties (e.g. hexagonal boron nitride (h-BN) or silicates)[17] suitable for printed and flexible electronics on-demand and in scale [18]. h-BN consists of a lattice of boron and nitrogen atoms arranged in a honeycomb structure [19]. Single-layer h-BN flakes have a wide bandgap of $\sim 6.47 \text{ eV}$, which is larger than their bulk counterpart (5.95 eV) [20]. The out-of-plane ϵ_r of h-BN is 3.29 and 3.76 for monolayer and bulk, respectively, which is comparable to that of SiO_2 (3.8) [21]. Moreover, inorganic h-BN offers better chemical stability against oxygen, moisture, and heat than organic dielectrics [22]. Inkjet printable dielectric inks with few-layer h-BN (FL h-BN) flakes and carboxymethyl cellulose (CMC) resulted in ϵ_r of ~ 7 and $B_v \sim 1 \text{ MV m}^{-1}$ [17], which falls in a similar range of polymer printable dielectrics.

However, printed dielectric films still suffer from a low B_v and the associated high leakage current, mostly due to the presence of pinholes and defects in the film. In addition, a manufacturing issue related to the roughness of these printed inks contributes to regions of high electric field density in the dielectric that may lead to breakdown. Another limitation reported, especially with the use of high boiling point solvents is the required annealing during printing or post-processing for solvent removal, which poses severe limitations when printing the inks on plastic or textile substrates [23, 24].

In this work we demonstrate water-based h-BN inkjet printable dielectric ink with $\epsilon_r \sim 16$, formulated by using 10% (in volume fraction to the exfoliated h-BN flakes) of BaTiO_3 nanoparticles as an additive, and show its viability for all-inkjet printed flexible capacitors with a capacitance of 10.39 nF cm^{-2} .

2. Experimental

2.1. Sample preparation

2.1.1. Hexagonal boron nitride (h-BN) ink formulation. 3 g of carboxymethyl cellulose sodium salt (CMC) (weight-average molecular weight, $M_w = 700\,000$, Sigma Aldrich, no. 419338) was added to 1 litre (1000 ml) of deionized water and was placed on a magnetic stirring plate overnight. Once the CMC was fully dissolved, 4 g of h-BN powder (Goodfellows B516011, $< 10 \mu\text{m}$ size) (concentration $\sim 4 \text{ mg ml}^{-1}$) was added to the solution and stirred until the solution became homogenized. The mixture was then microfluidized (M110-P Microfluidizer by Microfluidics) at a pressure of 200 MPa for 50 cycles. The h-BN ink was then centrifuged at 3000 rpm using a Thermo Fisher Scientific ultracentrifuge using a TH-641 swinging rotor for 20 min. The supernatant was carefully collected for further study.

2.1.2. Barium titanate (BaTiO_3) ink formulation. 3 mg ml^{-1} of CMC was added to deionized water and allowed to dissolve overnight with the aid of a magnetic stirrer. Once the CMC was dissolved, 10 mg ml^{-1} of BaTiO_3 nanopowder (cubic crystalline phase) (Sigma Aldrich, no. 467634) was added to the water-CMC mixture and then sonicated for 9 h (Fisherbrand FB15069, Max power 800 W). The BaTiO_3 ink was then centrifuged (Thermo Fisher Scientific ultracentrifuge using a TH-641 swinging) at 1000 rpm for 20 min. The supernatant was carefully collected for further study.

2.1.3. Hybrid h-BN and BaTiO_3 dielectric ink formulation. h-BN and BaTiO_3 inks were mixed in a volume ratio of 9:1 to form a hybrid BaTiO_3 /h-BN dielectric ink. Once the h-BN and BaTiO_3 inks were mixed in the appropriate ratio, the mixture was sonicated for 5 minutes allowing a homogeneous BaTiO_3 /h-BN ink to form.

2.1.4. Device architecture. Metal insulator metal (MIM) capacitor structures were used to characterize the dielectric ink. These are comprised of three different layers which were fabricated on a polyethylene terephthalate substrate. The first layer was made of a printed silver (Ag) film (Novacentrix JS-AS102A) with a dimension of $2.25 \text{ mm} \times 2.25 \text{ mm}$, this was followed by a dielectric layer which has $1.50 \text{ mm} \times 1.50 \text{ mm}$ dimension. Finally, the top layer was an Ag electrode of $0.5 \text{ mm} \times 0.5 \text{ mm}$ in size.

2.1.5. Inkjet printing. We used a drop on demand (DoD) Fujifilm Dimatix DMP-2800 inkjet printer mounting a Fujifilm DMC-11610 cartridge (nozzle diameter $\sim 21 \mu\text{m}$) to produce individual droplets with a volume of $\sim 10 \text{ pl}$. The platen temperature was switched off during the printing process and the cleaning cycle was set at 60 s. The Z number ($Z = \frac{1}{Oh} = \frac{\sqrt{\rho\gamma a}}{\eta}$) is the inverse of the Ohnesorge number (Oh) which is defined as $Oh = \frac{\eta}{\sqrt{\rho\gamma a}}$ where γ is the surface tension (mN m^{-1}), ρ is the density (g cm^{-3}), a is the diameter

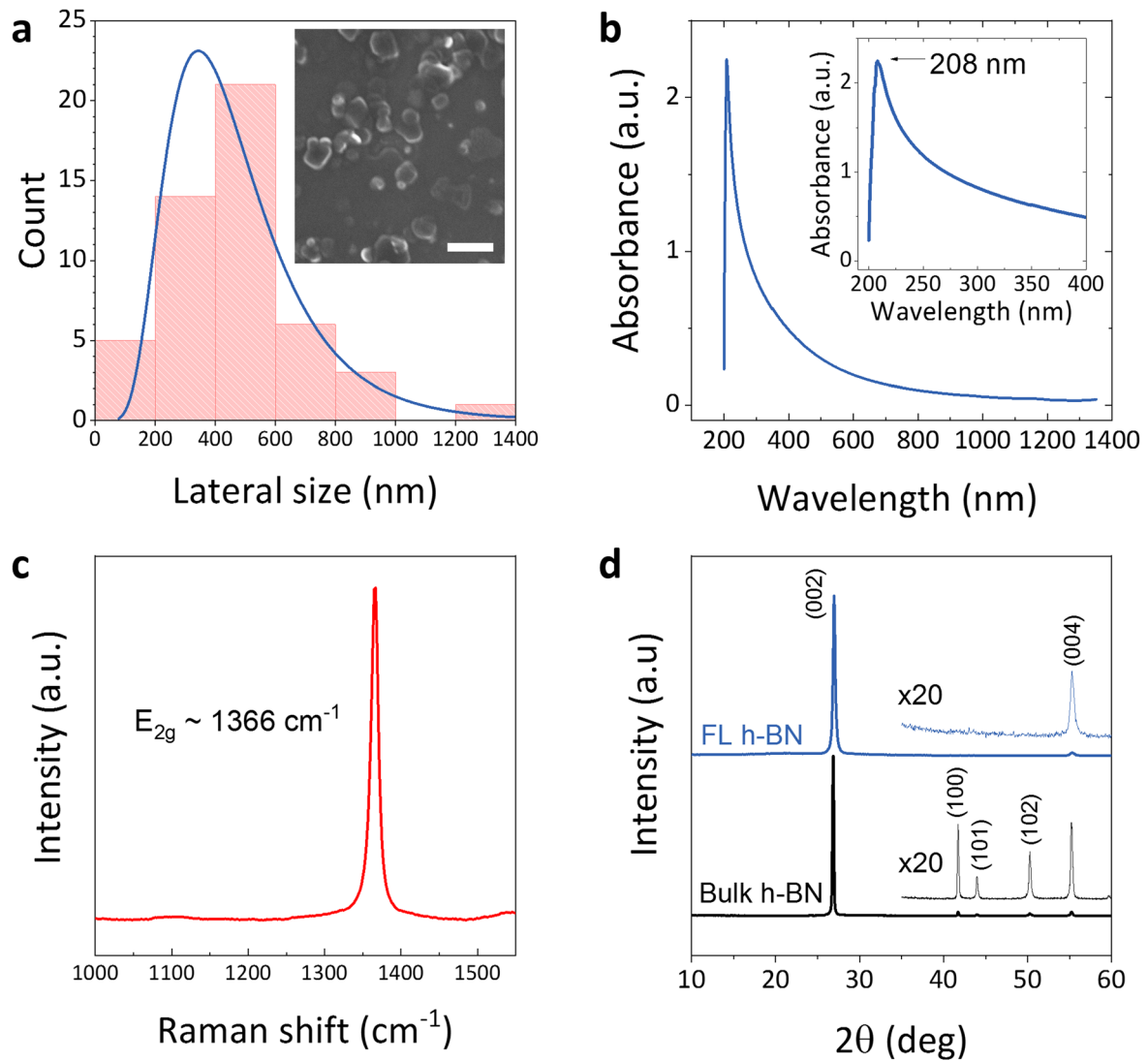


Figure 1. Characterization of the h-BN dispersion in aqueous solution of 3 mg ml^{-1} CMC. (a) Lateral size distribution of h-BN flakes. Inset is a SEM image of h-BN flakes printed from diluted ink. Scale bar is $1 \mu\text{m}$. (b) UV-vis absorption spectra of h-BN ink. Inset is shorter range plot near absorbance maxima. (c) Raman spectra of printed h-BN thin film. (d) XRD pattern of printed h-BN thin film and bulk powder.

of inkjet nozzle (μm), and η is the viscosity (mPa s). Ideally, inks suitable for inkjet printing need to have Z between 1 and 24 [17, 18]. The inter-drop distance is the space between two adjacent droplets that was measured from the centre of each drop after deposition. A uniform printed film is formed when the inter-drop distance is smaller than the drop diameter, and a uniform printed layer is formed as the drops merge without coalescing. The inter-drop distance for the bottom and top Ag electrodes in the MIM was $30 \mu\text{m}$, whereas the dielectric material was printed with an inter-drop distance of $10 \mu\text{m}$. Each Ag electrode was fabricated via 2 printing passes while the printing passes for the dielectric material was varied. The dielectric layers in the MIM devices were printed with 6, 8 and 10 printing passes. Three sets of MIM devices were made from h-BN, BaTiO_3 and hybrid h-BN/ BaTiO_3 .

2.1.6. Capacitance measurement. The capacitance of MIM capacitors was measured by a precision impedance analyzer (Agilent 4294) connected to a probe station (Cascade

Microtech Summit 12000). We used an equivalent series resistor-capacitor circuit to extract the capacitance from the impedance measurement [25]. The impedance amplitude is given by $|Z| = \sqrt{R^2 + (\omega C)^{-2}}$ where R is the series resistance, ω is the angular frequency, and C is the capacitance. The areal capacitance was calculated by dividing the capacitance (at 100 kHz) by the area of top electrode. The dielectric constant (ϵ_r) is calculated by $\epsilon_r = Ct/\epsilon_0 A$ where t is the thickness of dielectric layer, ϵ_0 is the dielectric permittivity of free space, and A is the top electrode area.

3. Results and discussions

3.1. h-BN ink

Figure 1(a) shows an SEM image (inset) and the statistics of the lateral sizes of obtained h-BN flakes. The log-normal

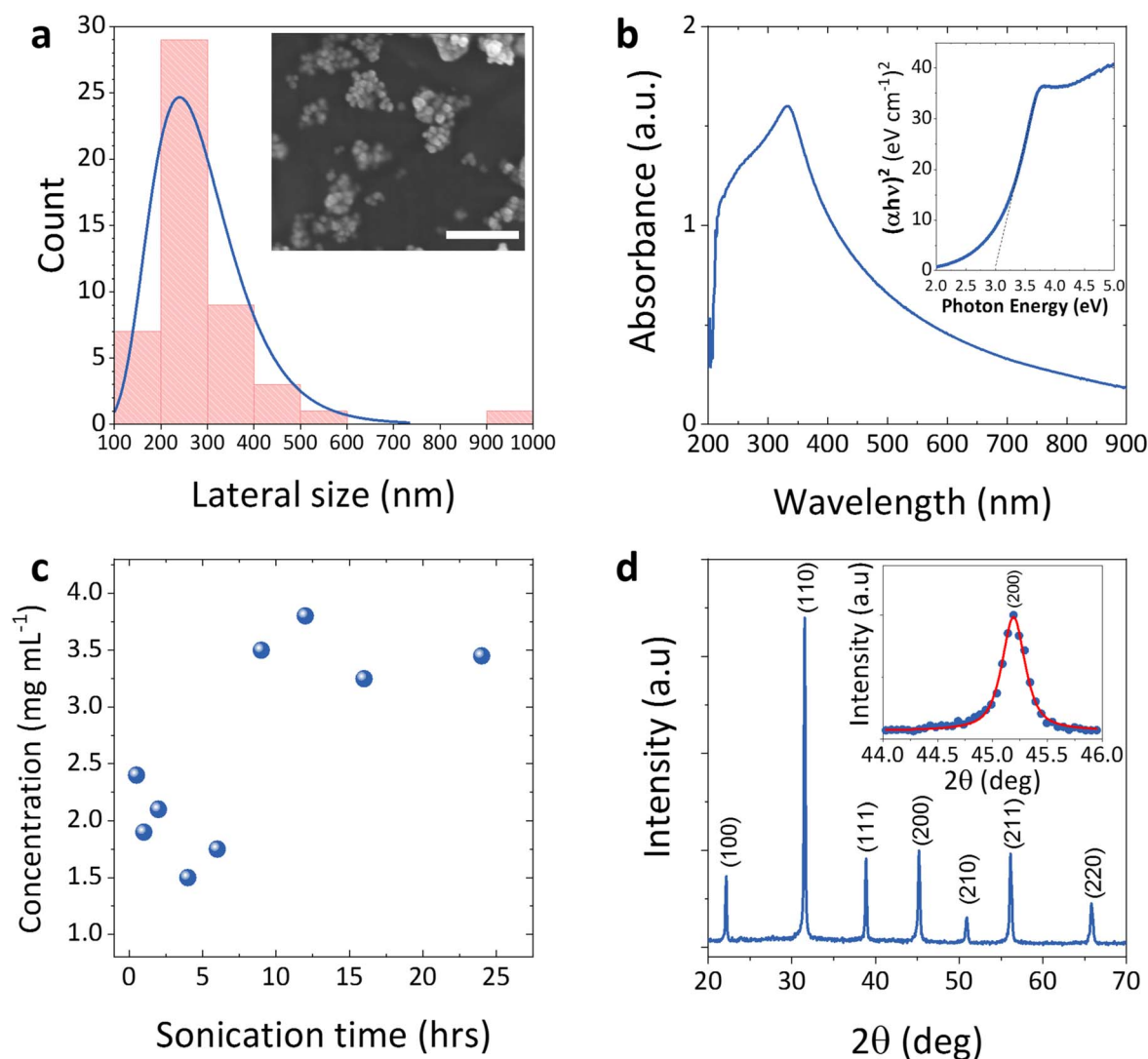


Figure 2. Characterization of the BaTiO₃ nanoparticle dispersion in aqueous solution of 3 mg ml⁻¹ CMC. (a) Lateral size distribution of BaTiO₃ nanoparticles. Inset is a SEM image of BaTiO₃ printed by diluted ink. Scale bar is 1 μm. (b) UV-vis absorption spectra of BaTiO₃ ink. Inset is corresponding Tauc plot, revealing an optical bandgap of 3.0 eV. (c) Concentration of BaTiO₃ inks as a function of ultrasonication time. Initial concentration is 10 mg ml⁻¹. (d) XRD pattern of printed BaTiO₃ film. Inset shows detailed (200) peak with Pseudo-Voigt fitting.

distribution is peaked at ~345 nm, which is in the same order of magnitude of printable h-BN inks previously reported [17]. The average particle size was ~60 times smaller than the nozzle diameter ($a = 21 \mu\text{m}$) of our printing cartridge, thus avoiding nozzle clogging. The morphology of h-BN flakes is shown in the inset SEM image. Figure 1(b) plots the UV-vis absorption spectra of FL h-BN ink with a peak centred at 208 nm (inset), which corresponds to intrinsic inter-band transition [26], revealing an optical band gap, E_g of ~5.96 eV. The Raman spectrum of h-BN ink deposited on a glass substrate is shown in figure 1(c) revealing a single peak at 1366 cm⁻¹ attributed to E_{2g} phonon vibrations, indicating that our h-BN flakes are few layers (3–5) thick [27] figure 1(d) shows the x-ray diffraction (XRD) curves of the h-BN ink (FL h-BN) deposited on a glass substrate compared to bulk h-BN powder. The absence of non-basal plane peaks such as (100), (101), and (102) suggests an excellent degree of exfoliation and restacking structure of h-BN flakes perpendicular to substrate normal [28, 29]. The h-BN flakes were

characterized by AFM (figure S1 (available online at stacks.iop.org/NANO/33/215704/mmedia)), where the log-normal distribution of flake thicknesses was found to be peaked at ~6 nm.

3.2. BaTiO₃ ink

Figure 2(a) shows the statistics of the size distribution of BaTiO₃ nanoparticles with the log-normal distribution peaked at 243 nm. The SEM image in the inset shows the morphology of BaTiO₃ nanoparticles that were printed from diluted ink. The UV-vis absorption spectrum of the BaTiO₃ ink is shown in figure 2(b). A smooth absorption edge is found which agree with literature [30], and the inset Tauc plot, extrapolation of linear onset of $(\alpha h\nu)^2$ versus $h\nu$ plot, reveals an optical band-gap of ~3.0 eV. The estimated optical band-gap is slightly smaller than that of bulk BaTiO₃ (3.2 eV), which can be attributed to band-gap narrowing in nanoparticles and strain [31]. It is worth noting that the absorption coefficients of BaTiO₃ nanoparticles

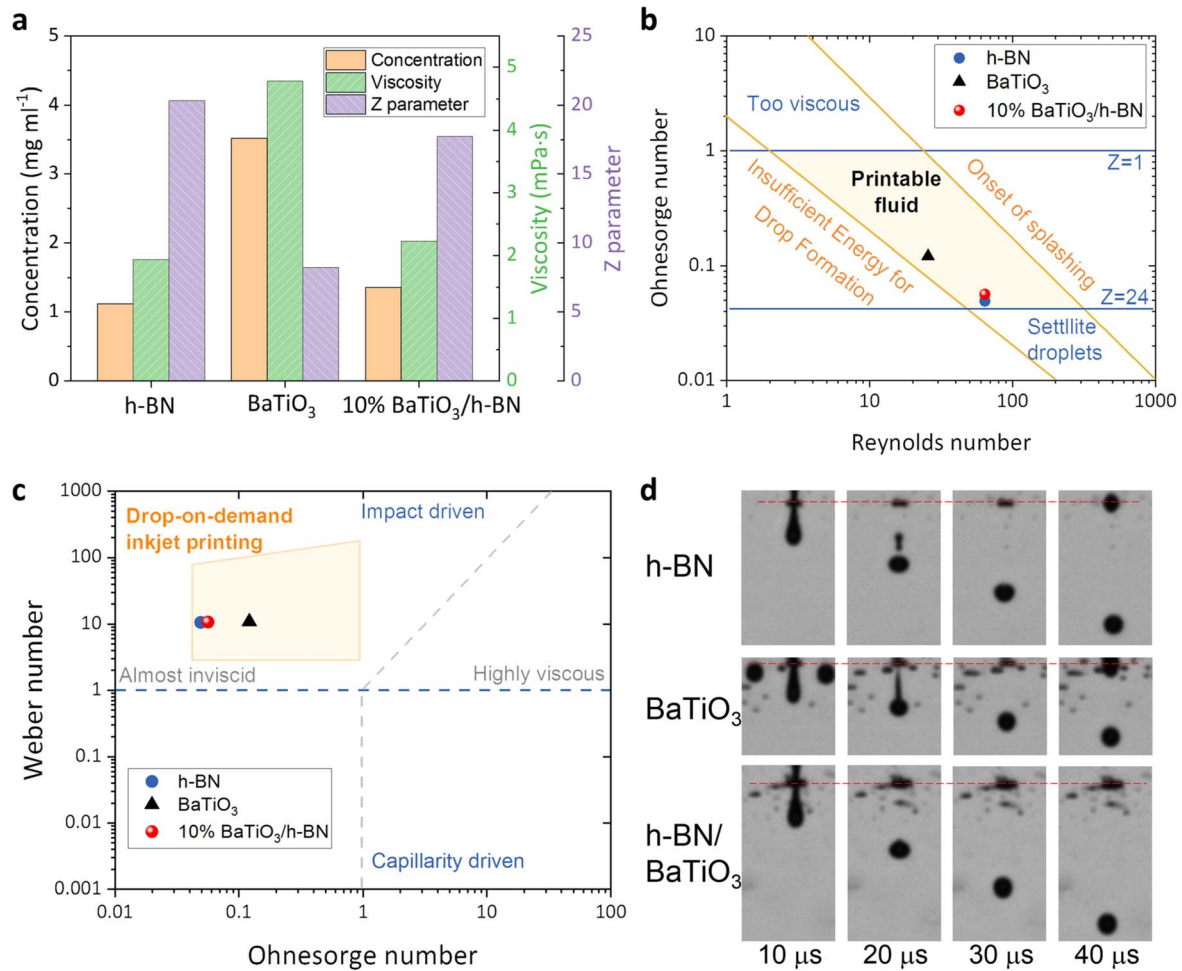


Figure 3. Comparison of h-BN, BaTiO₃, and 10% BaTiO₃/h-BN inks. (a) Concentration, infinite rate viscosity, and Z parameter plots. (b)–(c) Parameter mapping of (b) Reynolds and Ohnesorge numbers, and (c) Ohnesorge and Weber numbers of prepared inks in 3 mg ml⁻¹ CMC in water. (d) Optical microscopy images of inkjet-printed droplets for h-BN ink ($Z = 20.32$), BaTiO₃ ink ($Z = 8.25$), and 10% BaTiO₃/h-BN ink ($Z = 17.73$). Images were taken after jetting with the chosen delay (each row consists of 4 different droplets). Red dashed lines indicate the position of the nozzle. The droplet volume is 10 pl. The area above the red dashed line shows the reflection of the droplets.

are found to be $536.57 \text{ l g}^{-1} \text{ m}^{-1}$ and $241.39 \text{ l g}^{-1} \text{ m}^{-1}$ for the wavelengths of 660 and 1000 nm, respectively. To optimise the BaTiO₃ nanoparticle dispersion, different ultrasonication times were investigated for an initial concentration (c_i) of $\sim 10 \text{ mg ml}^{-1}$. As shown in figure 2(c), a sonication time of at least 9 h (followed by a centrifugation at 1000 rpm) is required to achieve a higher $c \sim 3.52 \text{ mg ml}^{-1}$, while shorter sonication times did not produce such a high concentration. The longer sonication time was not effective to increase concentration further. Figure 2(d) shows XRD spectra of printed BaTiO₃ thin film. The BaTiO₃ nanoparticle show high crystallinity despite of their small particle size. The inset shows detailed spectra for the (200) peak without distinct peak splitting, which confirms the cubic phase instead of tetragonal. The (200) peak center is found to be $2\theta = 45.19^\circ$ by fitting to Pseudo-Voigt function.

3.3. hybrid h-BN/BaTiO₃ ink

We investigate the evolution of the ϵ_r of the pure h-BN inks as a function of BaTiO₃ nanoparticles introduced in the dispersion. However, keeping the majority of dielectric material in

the ink in the form of flakes with a large aspect ratio maximises the stacking of the dispersed elements, while reducing the film thickness and the surface roughness in printed BaTiO₃/h-BN thin films. A rough surface may cause non-uniform dielectric performances and pin-holes or difficulty in printing as a function of multiple printing passes. Also, a highly rough surface may result in a very hydrophobic profile even though the nanosheet itself is hydrophilic, hindering drop coalescence and eventually preventing the formation of a uniform dielectric film [32]. For these reasons, in addition to h-BN and BaTiO₃ inks, we prepared a BaTiO₃/h-BN ink by blending h-BN and BaTiO₃ inks by keeping the volumetric ratio of h-BN flakes and BaTiO₃ nanoparticles in 9:1. Figure 3(a) summarizes and compares the characteristics of three inks in terms of concentration (c), viscosity (η) and Z parameters.

To determine the printability of the prepared inks, we first analysed the Z parameter which gives an indication of the jettability of a given ink from a nozzle (see methods). We determine the following rheological parameters: $\gamma_{\text{h-BN}} \sim 73.76 \text{ mN m}^{-1}$, $\rho_{\text{h-BN}} \sim 1.004 \text{ g cm}^{-3}$, $\eta_{\text{h-BN}} \sim 1.94 \text{ mPa}\cdot\text{s}$; $\gamma_{\text{BTO}} \sim 73.88 \text{ mN m}^{-1}$, $\rho_{\text{BTO}} \sim 1.007 \text{ g cm}^{-3}$, $\eta_{\text{BTO}} \sim 4.78$

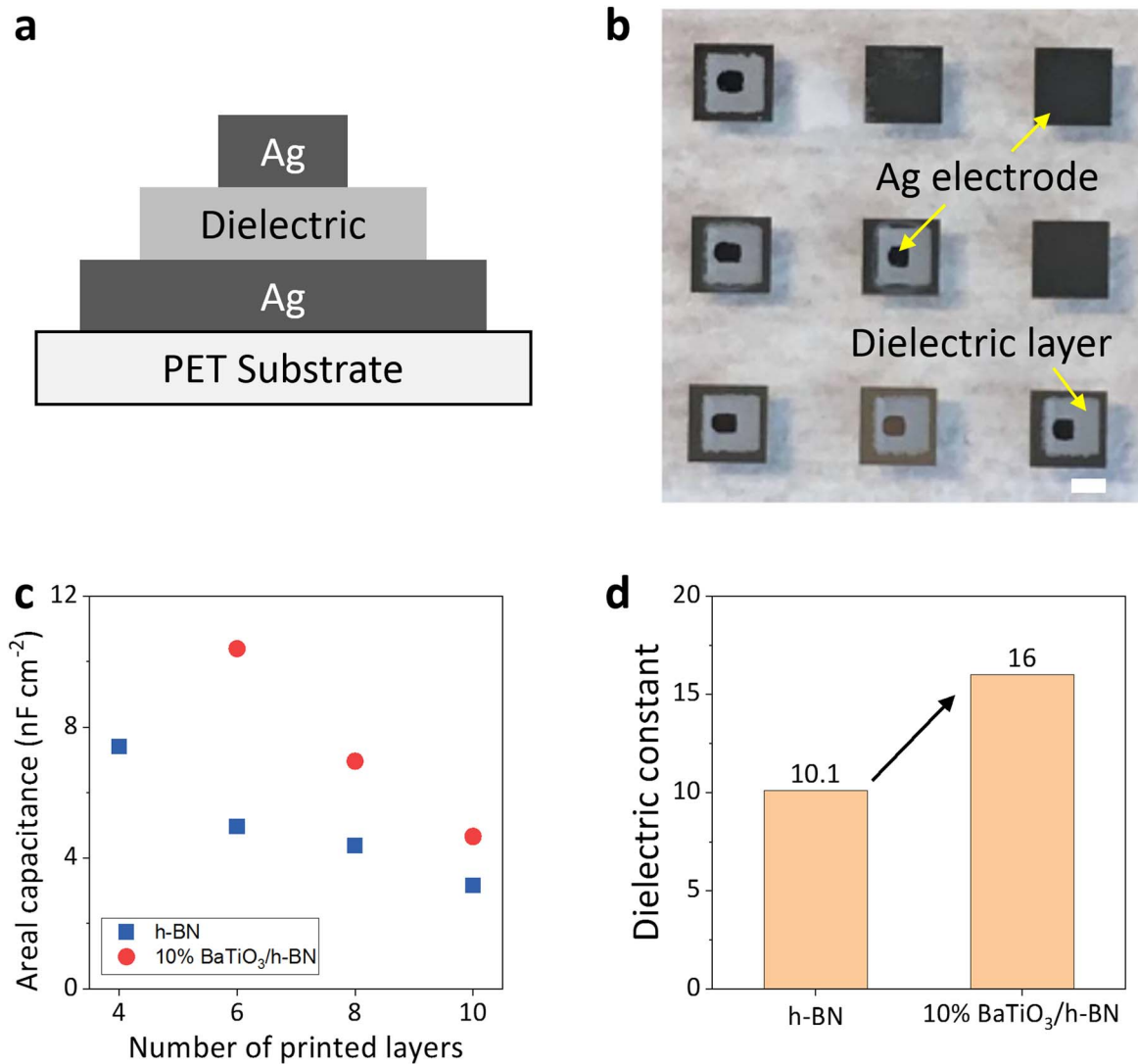


Figure 4. (a) Schematic side-view illustration of the printed MIM capacitor. (b) Optical microscope images of MIM capacitor array. Arrows denote the top and bottom Ag electrodes, and the dielectric layer between the Ag electrodes. Scale bar is 1mm. (c) Areal capacitance of the dielectric layers as a function of the number of printed layers. (d) Dielectric constants of h-BN thin films with and without 10% BaTiO₃ nanoparticles.

mPa·s; $\gamma_{\text{h-BN/BTO}} \sim 73.77 \text{ mN m}^{-1}$, $\rho_{\text{h-BN/BTO}} \sim 1.005 \text{ g cm}^{-3}$, $\eta_{\text{h-BN/BTO}} \sim 2.22 \text{ mPa}\cdot\text{s}$. Similar values were found for γ and ρ of the different inks, due to the dominant 3 mg ml^{-1} CMC in water as stabilizer. The Z parameters of h-BN, BaTiO₃, and 10% BaTiO₃/h-BN are 20.32, 8.25, and 17.73 respectively. The Ohnesorge number can be further divided into Weber number (We) and Reynolds number (Re): $Oh = (We)^{1/2}/Re$, $Re = V\rho a/\eta$, and $We = V^2\rho a/\gamma$, where V is the flow speed that is assumed as 6 m s^{-1} [33] figures 3(b) and (c) show the relationship between Re and Oh , and between Oh and We , respectively, showing that all three inks fits into the printable fluid regime. We draw the horizontal line for $1 < Z < 24$ that is defined as the optimal range for printing [17, 18]. Previous studies have discussed possible satellite droplets might occurred at $Z > 10$ [34, 35], we could notice such behaviour in the case of h-BN ink ($Z = 20.32$) but not in the 10% BaTiO₃/h-BN ink ($Z = 17.73$) (figure 3(d)).

All three inks meet the Z parameter requirement for successful printing. A small addition of BaTiO₃ ink into the h-BN ink resulted in a great modulation in the viscosity and Z parameter. The BaTiO₃/h-BN ink contains 1.01 mg ml^{-1} of h-BN and 0.35 mg ml^{-1} of BaTiO₃. Considering the density of nanomaterials (2.1 g cm^{-3} for h-BN, and 6.02 g cm^{-3} for BaTiO₃), the relative mass fraction of BaTiO₃ 34.6% corresponds to an equivalent volumetric fraction of 10.7%.

3.4. Inkjet-printed MIM capacitors

We have fabricated MIM capacitors to evaluate the dielectric performance of inkjet-printed thin films. Figure 4(a) shows the schematic cross-section of an all-printed MIM capacitor using silver and dielectric inks. Figure 4(b) shows the optical microscopy images of printed MIM devices. The dark squares correspond to the silver electrodes and white squares to the dielectric film. Figure 4(c) shows the areal capacitance (see

methods) of h-BN and 10% BaTiO₃/h-BN as a function of the number of printing passes for the dielectric film. A larger value of printing passes corresponds to a larger thickness of the dielectric thin film. Each printing pass increases the thickness of the printed thin film by approximately 270 nm (figure S2). The MIM capacitors with 10% BaTiO₃/h-BN dielectric layer have clearly higher areal capacitance than that of pristine h-BN/CMC dielectric layer. The former ranges from a 4.5 nF cm⁻² for 10 printing passes to 10 nF cm⁻² for 6 printing passes, while the latter ranges from 3.2 nF cm⁻² to 4.5 nF cm⁻² for the same printing conditions. This represents clear evidence that the 10% BaTiO₃ nanoparticle additive effectively boosts the dielectric performance of the printed h-BN film. As a result, the ε_r of the h-BN thin film of 10.1 has increased to 16.0 after embedding BaTiO₃ nanoparticles while keeping the inkjet printability (figure 4(d)). The breakdown voltages of the 10% BaTiO₃/h-BN capacitors with printing passes of 4, 6, and 8 are found to be 6.1 V, 14.9 V, and 32.6 V, respectively. The equivalent breakdown strengths are 6.3, 9.2, and 14.6 MV m⁻¹. The leakage current remained at the level of a few hundreds nA mm⁻² (figure S3).

The achieved enhancement of ε_r can be considered by Landauer's effective medium approximation (EMA) with the following equation [36]

$$x_1 \frac{(\rho_1 - \rho_m)}{(\rho_1 + 2\rho_m)} + x_2 \frac{(\rho_2 - \rho_m)}{(\rho_2 + 2\rho_m)} = 0,$$

where x_1 and x_2 are volumetric fraction of individual materials, ρ_1 and ρ_2 are material's property, and ρ_m is the approximated property of the mixture material. We can apply material 1 and 2 as h-BN/CMC and BaTiO₃/CMC, respectively, where $x_1 = 0.9$, $x_2 = 0.1$, $\rho_1 = 10.11$, and $\rho_2 = 430.81$. By using a quadratic formula for ρ_m , the effective solution for the dielectric constant of the mixture is calculated as 13.94 which is slightly smaller than the measured value of 16. This suggests that there could have been additional synergic effects occurring once the h-BN/BaTiO₃ film is formed. For example, the small gaps between the BaTiO₃ nanoparticles could have been filled by smaller FL h-BN.

4. Conclusions

We report an inkjet-printable water-based h-BN dielectric ink achieving a dielectric constant (ε_r) of 16.0. A 10% addition of BaTiO₃ nanoparticles into the h-BN/CMC dispersion results in an improvement of the dielectric constant by more than 50%, without altering the jetting ability. This result demonstrates that the hybrid combination of dielectric 2D materials and nanomaterials is a powerful route for the development of high-*k* printable dielectrics.

Acknowledgments

The authors acknowledge funding from EPSRC grants EP/P02534X/2, EP/R511547/1, EP/T005106/1, the Imperial College Collaboration Kick-Starter grant.

Data availability statement

The data that support the findings of this study will be openly available following an embargo at the following URL/DOI: <https://data.hpc.imperial.ac.uk/>. Data will be available from 1 February 2022.

ORCID iDs

Hyunho Kim  <https://orcid.org/0000-0003-2381-9716>

Benji Fenech-Salerno  <https://orcid.org/0000-0002-0150-9672>

Chengning Yao  <https://orcid.org/0000-0001-5446-8088>

Felice Torrisi  <https://orcid.org/0000-0002-6144-2916>

References

- [1] Khan Y, Thielens A, Muin S, Ting J, Baumbauer C and Arias A C 2020 *Adv. Mater.* **32** 1905279
- [2] Matsui H, Takeda Y and Tokito S 2019 *Org. Electron.* **75** 105432
- [3] Torrisi F and Carey T 2018 *Nano Today* **23** 73–96
- [4] Kim C, Wang Z M, Choi H J, Ha Y G, Facchetti A and Marks T J 2008 *J. Am. Chem. Soc.* **130** 6867–78
- [5] Buchheit R, Kuttich B, Gonzalez-Garcia L and Kraus T 2021 *Adv. Mater.* **33** 2103087
- [6] Yang K, Huang X Y, Huang Y H, Xie L Y and Jiang P K 2013 *Chem. Mater.* **25** 2327–38
- [7] Petrovsky V, Petrovsky T, Kamlapurkar S and Dogan F 2008 *J. Am. Ceram. Soc.* **91** 3590–2
- [8] Zhang Y C, Wang X H, Kim J Y, Tian Z B, Fang J, Hur K H and Li L T 2012 *J. Am. Ceram. Soc.* **95** 1628–33
- [9] Torrisi F and Coleman J N 2014 *Nat. Nanotechnol.* **9** 738–9
- [10] Piatti E et al 2021 *Nat. Electron.* **4** 893–905
- [11] Hernandez Y et al 2008 *Nat. Nanotechnol.* **3** 563–8
- [12] Karagiannidis P G et al 2017 *ACS. Nano* **11** 2742–55
- [13] Su C Y, Lu A Y, Xu Y P, Chen F R, Khlobystov A N and Li L J 2011 *ACS. Nano* **5** 2332–9
- [14] Zhang C F et al 2019 *Nat. Commun.* **10** 1795
- [15] Kelly A G et al 2017 *Science* **356** 69–72
- [16] Carey T et al 2021 *Adv. Electron. Mater.* **7** 2100112
- [17] Carey T, Cacovich S, Divitini G, Ren J S, Mansouri A, Kim J M, Wang C X, Ducati C, Sordan R and Torrisi F 2017 *Nat. Commun.* **8** 1202
- [18] Torrisi F et al 2012 *ACS Nano* **6** 2992–3006
- [19] Golberg D, Bando Y, Huang Y, Terao T, Mitome M, Tang C and Zhi C Y 2010 *ACS Nano* **4** 2979–93
- [20] Wickramaratne D, Weston L and Van de Walle C G 2018 *J. Phys. Chem. C* **122** 25524–9
- [21] Laturia A, Van de Put M L and Vandenberghe W G 2018 *Npj 2d Mater. Appl.* **2** 6
- [22] Brebels J, Manca J V, Lutsen L, Vanderzande D and Maes W 2017 *J. Mater. Chem. A* **5** 24037–50
- [23] Ren J S, Wang C X, Zhang X, Carey T, Chen K L, Yin Y J and Torrisi F 2017 *Carbon* **111** 622–30
- [24] Ji X Q, Liu W W, Yin Y J, Wang C X and Torrisi F 2020 *J. Mater. Chem. C* **8** 15788–94
- [25] Kelly A G, Finn D, Harvey A, Hallam T and Coleman J N 2016 *Appl. Phys. Lett.* **109** 023107
- [26] Hoffman D M, Doll G L and Eklund P C 1984 *Phys. Rev. B* **30** 6051–6
- [27] Gorbachev R V et al 2011 *Small* **7** 465–8

- [28] Li L H, Chen Y, Behan G, Zhang H Z, Petravic M and Glushenkov A M 2011 *J. Mater. Chem.* **21** 11862–6
- [29] Li L H, Chen Y, Cheng B M, Lin M Y, Chou S L and Peng Y C 2012 *Appl. Phys. Lett.* **100** 261108
- [30] Khan M A M, Kumar S, Ahamed M, Ahmed J, Kumar A and Shar M A 2021 *J. Mater. Sci-Mater. El.* **32** 12911–21
- [31] Ramakanth S and Raju K C J 2014 *J. Appl. Phys.* **115** 173507
- [32] Zhao M Q, Xie X Q, Ren C E, Makaryan T, Anasori B, Wang G X and Gogotsi Y 2017 *Adv. Mater.* **29** 1702410
- [33] Chuang M Y 2017 Inkjet printing of Ag nanoparticles using dimatix inkjet printer, No 2, protocols and reports. Paper 40. and (http://repository.upenn.edu/scn_protocols/40)
- [34] Derby B 2011 *J. Eur. Ceram. Soc.* **31** 2543–50
- [35] Maleki H and Bertola V 2020 *Catal. Sci. Technol.* **10** 3140–59
- [36] Landauer R 1952 *J. Appl. Phys.* **23** 779